

## Temperature variation and solution treatment of high strength AA7050

LI Pei-yue<sup>1,2</sup>, XIONG Bai-qing<sup>2</sup>, ZHANG Yong-an<sup>2</sup>, LI Zhi-hui<sup>2</sup>

1. Luoyang Ship Material Research Institute, Luoyang 471003, China;

2 State Key Laboratory of Nonferrous Metals and Processes,  
General Research Institute for Nonferrous Metals, Beijing 100088, China

Received 3 March 2011; accepted 26 October 2011

**Abstract:** Temperature variation and solution treatment of high strength aluminum alloy were investigated with temperature data acquisition system, microstructural observation, mechanical properties test, electrical conductivity measurement and differential scanning calorimetry (DSC) analysis. Specimens with two dimensions were employed in the experiment. The results indicate that the specimens with large size undergo low solution temperature and short time, giving rise to the reduction of hardening precipitates. The optimized solution treatments for specimens with dimensions of 25 mm×25 mm×2.5 mm and 70 mm×60 mm×20 mm are (480 °C, 30 min) and (480 °C, 90 min), respectively. The densities of GP zones and  $\eta'$  phases of the small specimen are higher than those of the large specimen, which is consistent with the properties of the alloys.

**Key words:** aluminum alloy; specimen size; solution treatment; heating rate; hardening precipitate

### 1 Introduction

Al–Zn–Mg–Cu aluminum alloys (7000 series) are extensively used in aerospace applications for their high mechanical properties, damage tolerance and good corrosion resistance [1,2]. 7000 series aluminum alloys are aging hardening alloys, whose properties are determined by the coherent or semi-coherent precipitates formed during aging treatment [1,3,4]. The quantity of hardening precipitates increases with supersaturation of the quenched solution. Optimizing solution treatment can be as effective as adding elements to raise the solution saturation. Meanwhile, the volume and size of the residual second phases decrease obviously, which will improve the ductility [5,6].

Thick plates of 7000 series pre-stretched and forged aluminum alloys have been used extensively in aircraft and aerospace industry recently [7–9]. Quenching sensitivity, which restricts the development of component size, exists massively in the 7000 series alloys [4,10–12]. The variance in tensile strength between center and surface of the plate is up to 15% for 7050 (Al–6.2Zn–2.3Mg–2.3Cu–0.12Zr) alloy with 120 mm in thickness mainly caused by the cooling rate

discrepancy [1]. In recent years, numerous experiments focused on the solution process of 7000 series alloys have been carried out [5,6]. However, investigations on temperature variation and the effect of specimen sizes on solution treatment of high strength aluminum alloy are rather limited. Temperature variation in the solution and quenching processes is vital to the quenching sensitivity, but little research has been done about it. The present work aims to arrive at a detailed understanding of the effects of specimen sizes on the heating and cooling rates, and on the solid solution treatment.

### 2 Experimental

The composition of AA7050 is detailed in Table 1. As-rolled thick plates were received from Northeast Light Alloy Co., Ltd., China. These blocks were 340 mm in length and had cross sections of 1200 mm (LT) × 60 mm (ST). Specimens were hanged in a muffle furnace during the solution treatment process. Specimen I (70 mm×60 mm×20 mm) and specimen II (25 mm×25 mm×2.5 mm) were selected at quarter thickness of the plate, in order to ensure a maximum homogeneity of composition and grain structure.

**Table 1** Chemical composition of alloy (mass fraction, %)

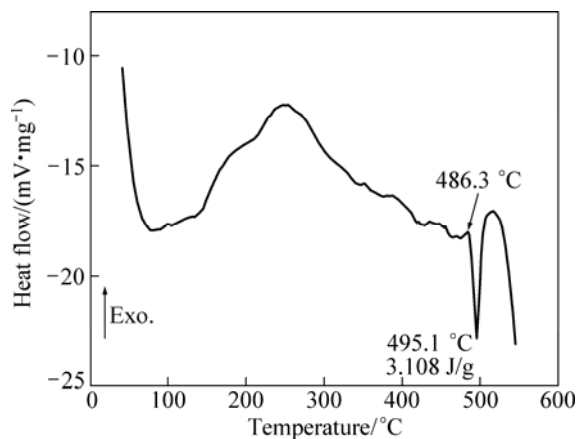
Zn	Mg	Cu	Zr	Fe	Si	Mn	Cr	Ti	Al
5.93	2.23	2.16	0.11	0.068	0.019	<0.01	<0.01	0.020	Bal.

The hardness was determined under load of 10 N in a 430–SVD Vickers hardness meter. Electrical conductivity was measured on a WD-Z digital eddy current conductivity meter. This meter (measuring in unit of %IACS) was calibrated with a test block to the requirements of ASTM E92–82 [13]. Tensile testing was performed on MTS–810 in accordance with ASTM B557–84 [14]. Specimens were tested at a strain rate of 1–2 mm/min. Specimens had a K-type thermocouple with 1.5 mm in diameter inserted from one end so that its tip was at the mid-point of the specimen. Specimens were subsequently solution heat-treated at different temperatures and quenched into water. The heating and cooling curves were monitored at 100 Hz using a MX100 data acquisition system. Microstructure was investigated on a Zeiss Axiovert 200MAT optical microscope (OM) and HITACHI S4800 scanning electron microscope (SEM). OM specimens were polished and etched in Graff Sergeant’s reagent (84 mL water, 15.5 mL HNO<sub>3</sub>, 0.5 mL HF, 3 g CrO<sub>3</sub>) to show the grain structure. The fraction of residual secondary phases was measured by image-pro plus & analyzer. Differential scanning calorimetry (DSC) was conducted on NET ZSCH STA 409 C/CD thermal analyzer with heating rate of 10 °C/min, under the argon gas condition.

### 3 Results and discussion

#### 3.1 Temperature variation

The DSC technique has been used in many investigations to characterize the solid state reactions accompanying the dissolution of precipitates, as well as the formation of addition precipitates [15,16]. Figure 1 shows the DSC thermogram of the as-rolled AA7050. The endothermic peak around 490 °C could be ascribed

**Fig. 1** DSC thermogram for as-rolled AA7050

to the dissolution of eutectic phases. The DSC profile reveals that the thermal behavior of the overburning temperature was almost 486.3 °C, which indicates that the upper temperature limit for the alloy treated by conventional solution treatment is 486.3 °C.

Figure 2 shows the heating and cooling curves of the specimens during solution treatment and quenching processes. It takes 70, 80 and 140 min for specimen I to reach 450 °C, 460 °C, 475 °C, respectively (Fig. 2(a)). The temperature of the specimen I is about 5 °C lower than that of the furnace in the experiment. The heat transferring was mainly conducted by air in the muffle furnace. The less the difference between the specimen and air was, the slower the heat exchange was, until they reached a dynamic balance. In Fig. 2(b)), the cooling curve of specimen I quenched with water shows that it takes 6 s for the specimen to reach 182.9 °C from the solution temperature. And the average cooling rate can reach 58.8 °C/s. In Fig. 2(c)), it can be seen obviously that the small specimen can reach the solution temperature in 5 min. The average cooling rate of specimen II is up to 300 °C/s (Fig. 2(d)).

The temperature evolution can be explained as follows.

The heat absorbed in a temperature field for an object is

$$Q=qA \quad (1)$$

where  $Q$  is the heat transferred;  $q$  is the heat flow density;  $A$  is the surface area. Equation (1) can be written as:

$$Q=cm\Delta t=c\rho V\Delta t \quad (2)$$

where  $c$  is the specific heat capacity;  $m$  is the mass;  $\rho$  is the density;  $V$  is the volume;  $\Delta t$  is temperature variation. Comparing Eqs. (1) with (2), then we get

$$qA=c\rho V\Delta t \quad (3)$$

Equation (3) above becomes

$$\Delta t = qA/(c\rho V) = \frac{A}{V} \cdot \frac{q}{c\rho} \quad (4)$$

Finally, a ratio representing the linear relationship between  $\Delta T$  and  $\Delta t$  is obtained as:

$$R = \frac{\partial T}{\partial t} = \frac{A}{V} \cdot \frac{1}{c\rho} \cdot \frac{\partial q}{\partial t} \quad (5)$$

where  $R$  is the heating rate.

When treating in the same furnace,  $R$  is proportional to the ratio of  $A/V$  for specimens I and II.

$$R_{\text{I}} = \left( \frac{A}{V} \right)_{\text{I}} = 0.162$$

$$R_{\text{II}} = \left( \frac{A}{V} \right)_{\text{II}} = 0.96$$

$$R_{\text{II}}:R_{\text{I}}=5.926$$

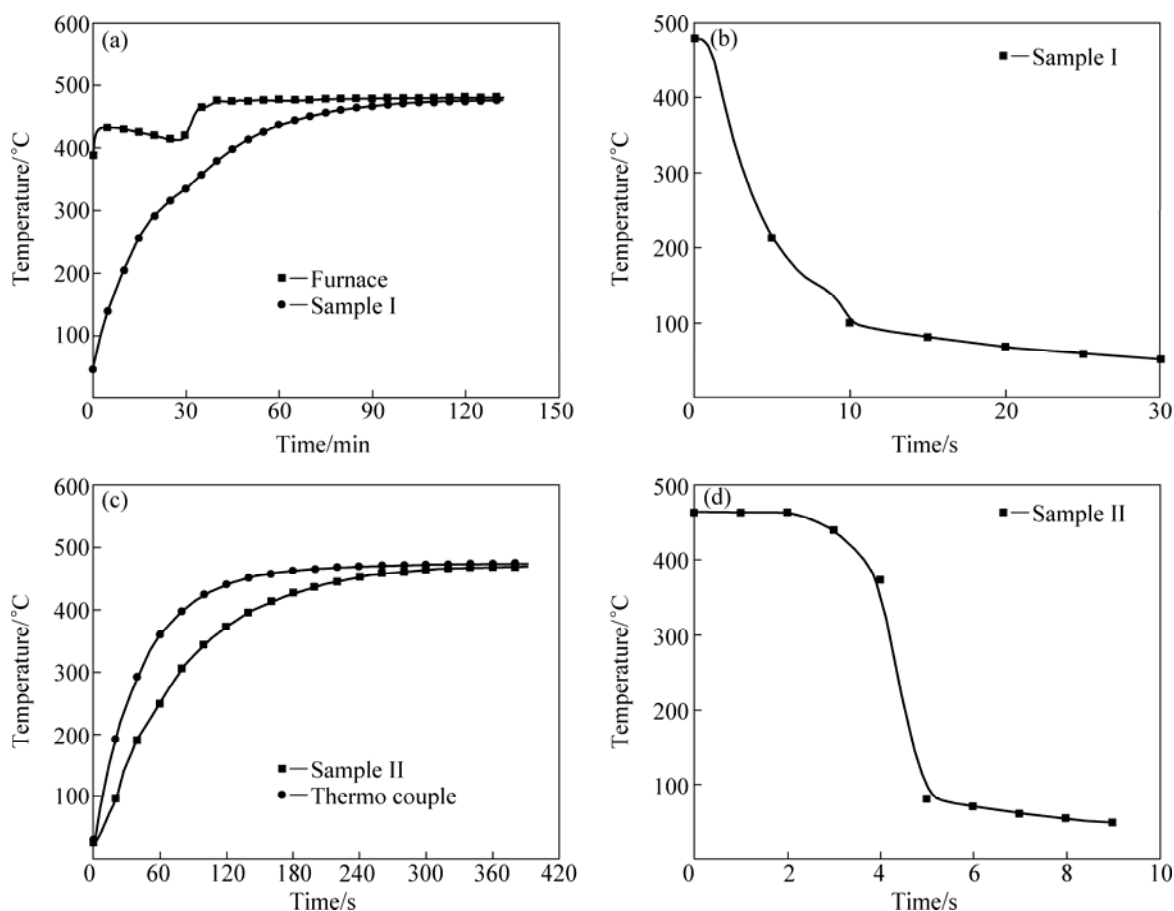


**Fig. 2** Heating and cooling curves of specimens I (a, b) and II (c, d) during solid solution at 480 °C and quenching processes: (a), (c) Heating curves; (b), (d) Cooling curves

The heating rate of specimen II is about 6 times that of the specimen I. Specimen I could reach 460 °C within 80 min when solid solution treated at 480 °C, while it took only 5 min to arrive at 480 °C for specimen II.

There are differences of power and temperature distribution for various solid solution furnace and aging equipment, which will lead to distinct temperature and heating rate. Differences of effective heat treatment temperature and time will result in lower test repeatability when the specimen with different sizes was treated in the same furnace. Furthermore, the cooling curves are different in quenching process for different size specimens. Specimen I (70 mm×60 mm×20 mm) and specimen II (25 mm×25 mm×2.5 mm) were used to establish the solution treatment process.

### 3.2 Solution treatment

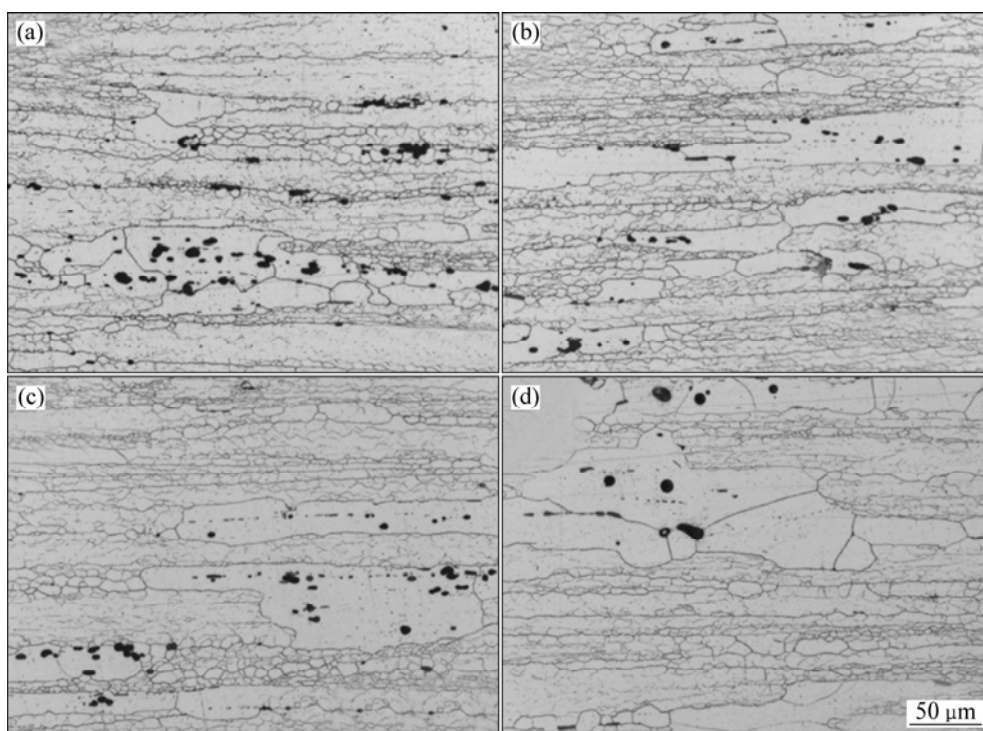
#### 3.2.1 Specimen I (70 mm×60 mm×20 mm)

In Fig. 3, the optical microstructures of specimen I solution treated at different temperatures are revealed by Graff Sargent's reagent. The growing of the grain size and gradual decrease of residual phase's fraction with increasing the solution temperature was evident. Serious

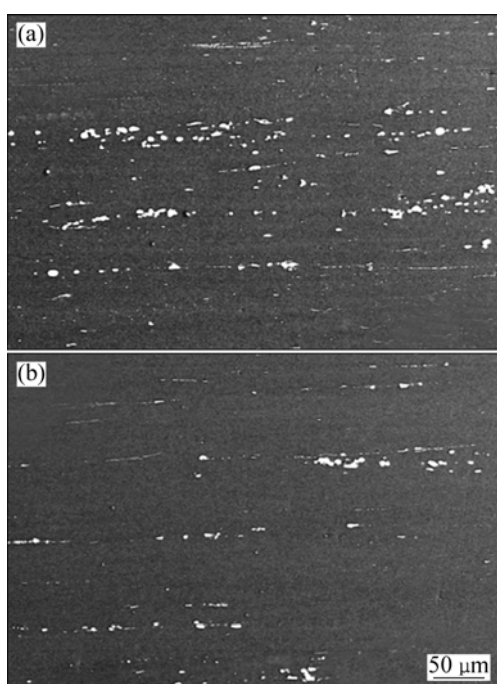
overburning was observed after solution heat treatment at 495 °C.

Figure 4 displays the BSE image showing typical solution heat treated microstructure of the alloy. The decrease of residual phase is evident in the micrograph. Figure 5 shows the residual phase area fraction of the solid solution heat treated alloy. It can be found that the residual phase area fraction declined with increasing the solid solution temperature. It appears that the fraction decreased substantially in the temperature range of 465–480 °C, and reached a slow decreased stage with increasing the solution temperature.

Figure 6 shows the influence of solution heat treatment temperature on the hardness, electrical conductivity and mechanical properties of the alloy. From Figs. 6(a) and (c), it can be found that the hardness and strength reached a maximum value after solution treatment at 485 °C. From Fig. 6(b), it can be seen that the electrical conductivity decreased rapidly at higher solution temperatures, indicating that the solution temperature had a dominant role in dissolution of the residual second phases. With increasing solution temperature from 485 to 505 °C, the elongation,  $A$ ,



**Fig. 3** Optical microstructures of specimen I solution treated at different temperatures for 1 h: (a) 465 °C; (b) 475 °C; (c) 485 °C; (d) 495 °C



**Fig. 4** SEM images of specimen I solution treated at different temperatures for 1 h: (a) 465 °C; (b) 475 °C

decreased markedly as a consequence of overburning. Considering the DSC result, the optimal solid solution treatment temperature is 480 °C for specimen I.

Figure 7 shows the optical microstructures of the specimen I solution treated at 480 °C for various time. It

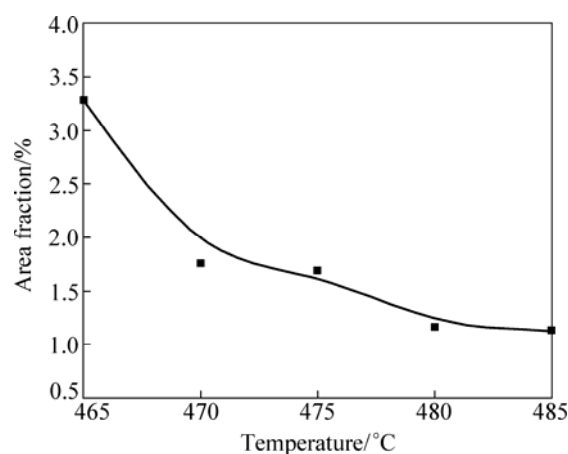


**Fig. 5** Area fraction of residual second phases in specimen I solution treated at different temperatures for 1 h

can be seen that the second phases dissolved rapidly in the first 90 min, as shown in Figs. 7(a)–(c). Recrystallization was obvious after solution treatment for 120 min.

Figure 8 shows the effects of solution treatment time on hardness, electrical conductivity and mechanical properties of the alloy in T6 temper. It can be seen that the solution time had a little effect on the hardness and mechanical properties of the alloy. From Fig. 8(b) it can be observed that the electrical conductivity decreased gradually before a plateau is observed at 120 min. Considering the effect of solution time on the

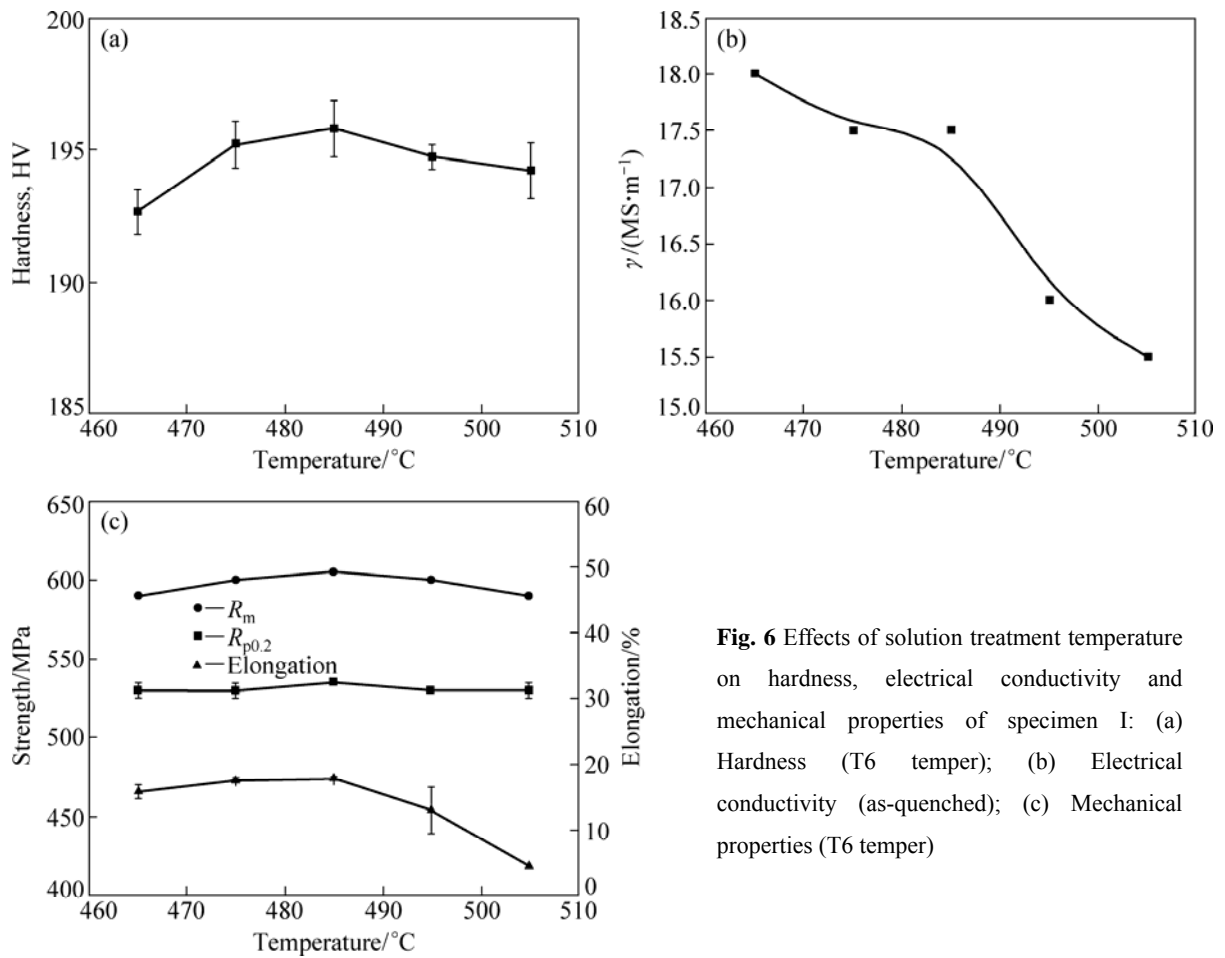


**Fig. 6** Effects of solution treatment temperature on hardness, electrical conductivity and mechanical properties of specimen I: (a) Hardness (T6 temper); (b) Electrical conductivity (as-quenched); (c) Mechanical properties (T6 temper)

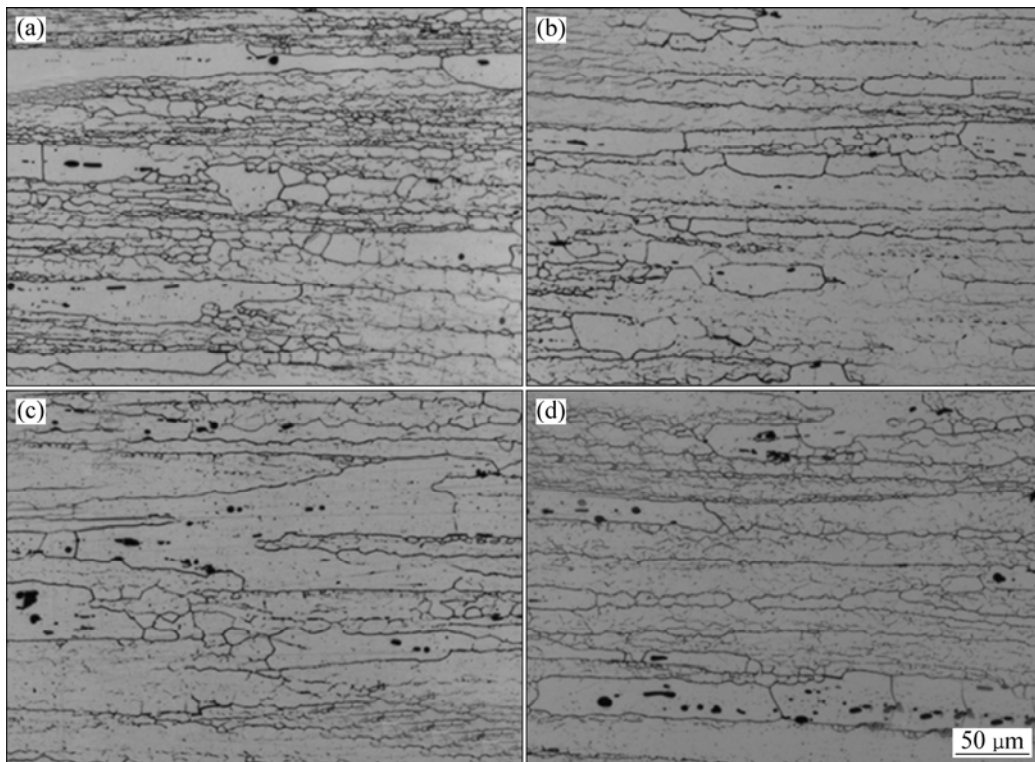


**Fig. 7** Optical microstructures of specimen I solution treated at 480 °C for various time: (a) 30 min; (b) 60 min; (c) 90 min; (d) 120 min

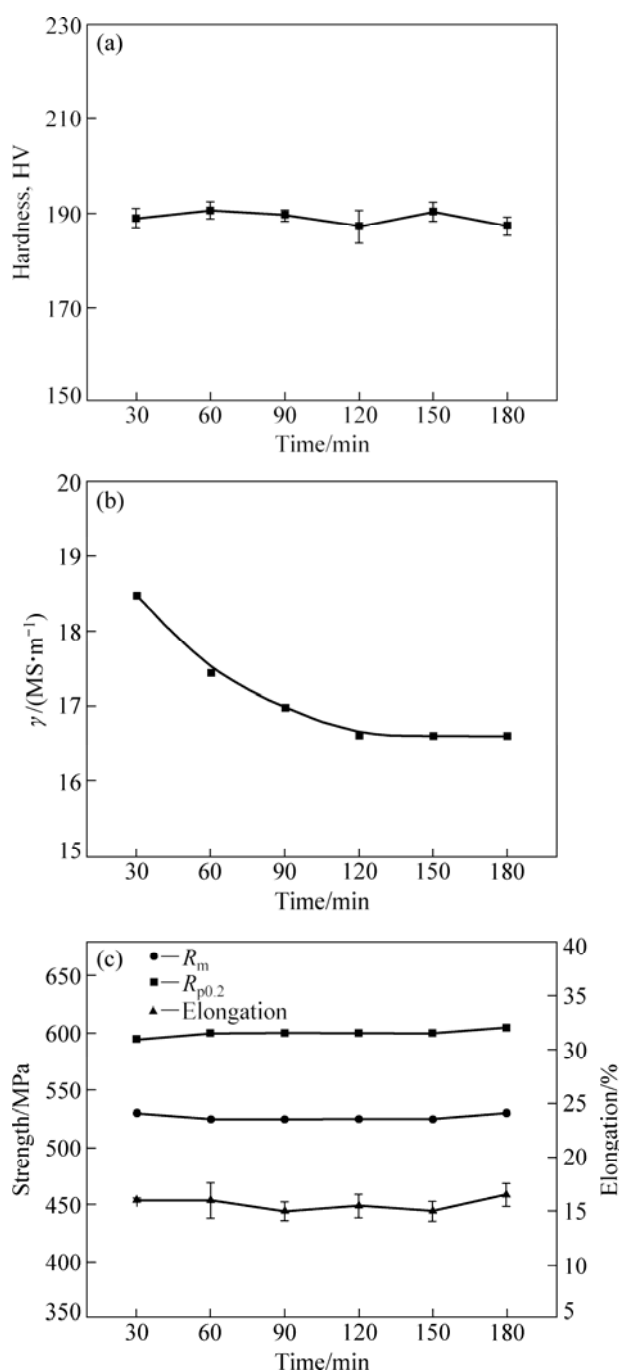


**Fig. 8** Effects of solution treatment time on hardness, mechanical properties and electrical conductivity of specimen I: (a) Hardness (T6 temper); (b) Electrical conductivity (as-quenched); (c) Mechanical properties (T6 temper)

microstructure, the reasonable solution time is 90 min. So, the optimal solid solution treatment is at 480 °C for 90 min for specimen I.

### 3.2.2 Specimen II (25 mm×25 mm×2.5 mm)

Figures 9 and 10 show the influence of solution treatment on the hardness and electrical conductivity of specimen II, respectively. In Fig. 9(a), it can be seen that the hardness reached the maximum value at after

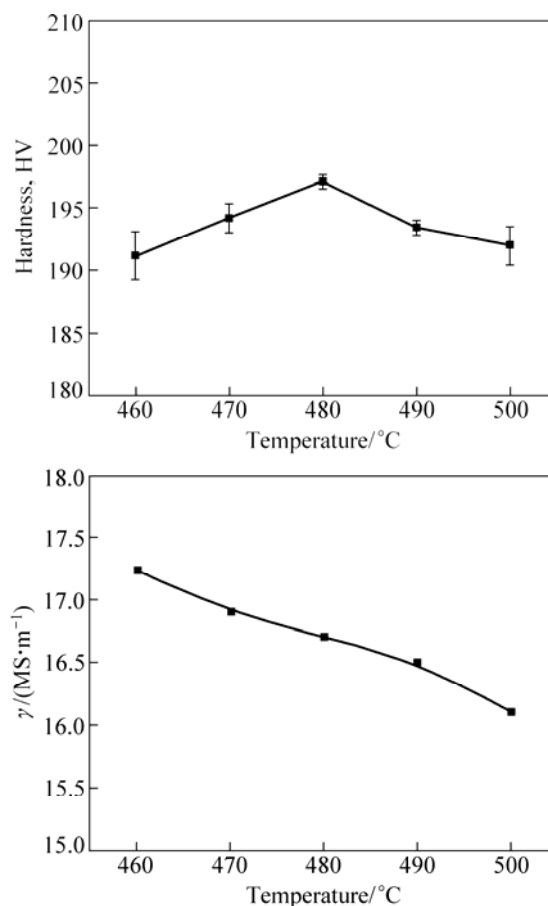


**Fig. 9** Influence of solution temperature on hardness and electrical conductivity of specimen II: (a) Hardness; (b) Electrical conductivity

treatment 480 °C for 60 min. From Fig. 9(b), it can be found that the electrical conductivity decreased continuously with the increase of solution temperature. As shown in Fig. 10, the solution time had little influence on the hardness and electrical conductivity. These implied that the optimal solid solution treatment for specimen II is at 480 °C for 30 min.

Typical DSC thermograms were obtained after aging treatment and compared with the thermograms of the alloy in as-rolled condition. Figure 11 shows that the exothermic peak of eutectic phases around 490 °C shifts downwards compared with that of the as-rolled plate, which suggests that the dissolution of eutectic phases took place. The peaks evolved in 100–300 °C showing key dissolution and precipitation events are consistent with other works [15–17]. The endothermic peak *A* revealed the relevant reactions of the GP zones and  $\eta'$  phases, which determines the strength of the alloy. It can be found that the specimen II had a higher amount of peak *A* than specimen I. The exothermic peaks *B* and *C* correspond to the two main reactions of  $\eta'$  formation and growth and  $\eta$  formation. It can be found that more GP

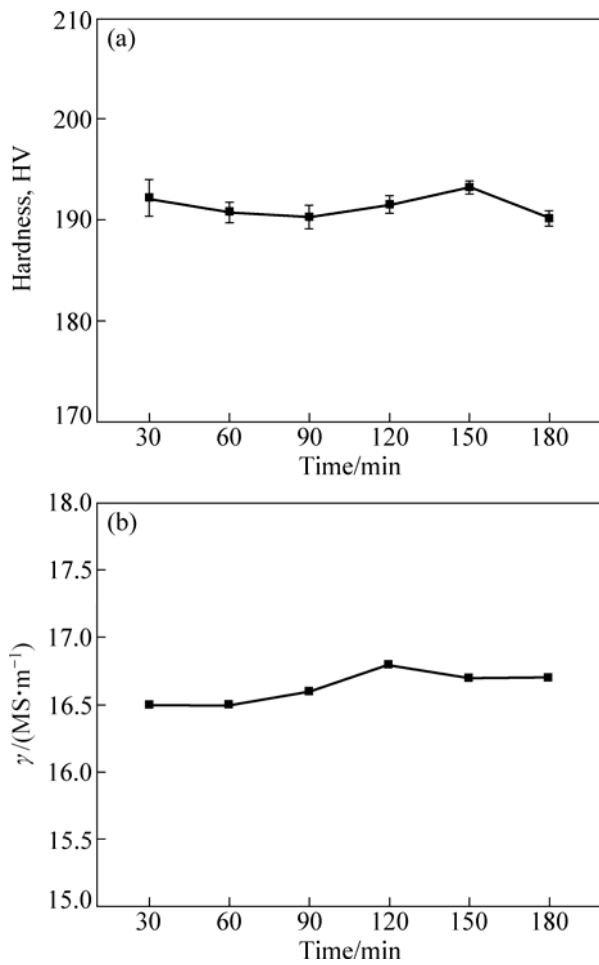


Fig. 10 Influence of solution time on hardness and electrical conductivity of specimen II: (a) Hardness; (b) Electrical conductivity

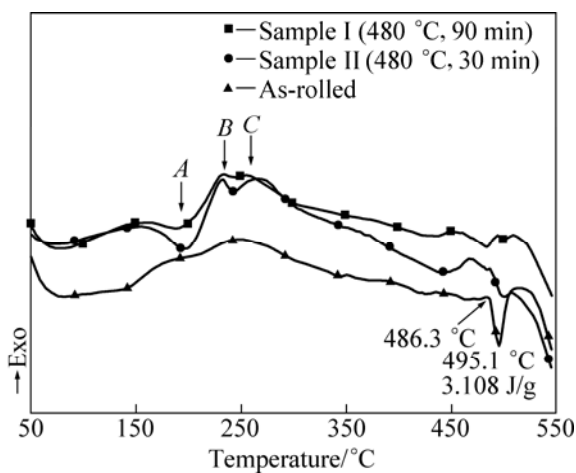


Fig. 11 Effect of specimen size on DSC thermograms of alloy (T6 temper for specimens I and II)

zones and  $\eta'$  phases formed in specimen II. These indicate that solid solution supersaturation of specimen II was higher than that of the specimen I, which is consistent with the properties of the alloys.

It can be found that the small size specimen underwent higher solution temperature and longer time than the large specimen during the solution treatment. Solution treatment is the key process of high strength aluminum alloys, which makes the alloy elements go back to the matrix to produce supersaturated solid solution. The supersaturation of the solid solution can be influenced by the solution temperature, holding time and cooling rate. And the solution temperature is the dominant factor. The supersaturation in the grains will augment with the enhancement of the solution temperature [18]. Thermodynamics analysis indicates that the driving force of precipitation is larger when the solution elements increase. The effect of supersaturation degree on the free energy of precipitation during the aging treatment is shown in Fig. 12 [19].  $G_\alpha$  and  $G_\beta$  in Fig. 12 are the free energy—chemical curves of the matrix and precipitates. When we improve the solution temperature or prolong the solution time, the elements in the matrix increase to  $C_0'$  from  $C_0$ , which makes the precipitation driving force of the  $\beta$  phases increase to  $G_1'-G_2'$ . It is obvious  $G_1'-G_2'$  is bigger than  $G_1-G_2$ . From the nucleation theory, the critical radius of the nucleation is inverse relation to the Gibbs free energy. So, the higher the supersaturation degree, the lower the Gibbs free energy of the system. The critical radius of the nucleation becomes small and the nucleation rate will be higher, which will produce abundant fine aging precipitation to enhance the aging strengthening.

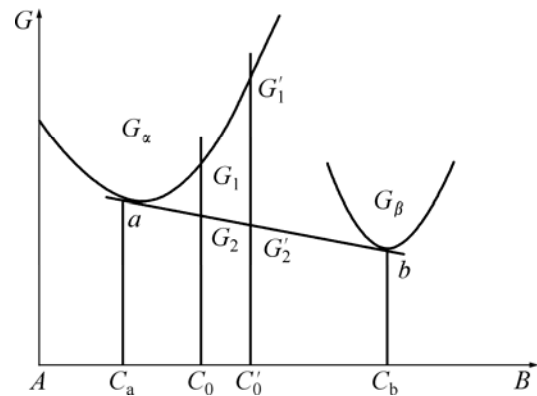


Fig. 12 Free energy change of precipitation under different supersaturation condition [20]

But the grains grow with the augment of solution temperature and time. Hall-Petch relationship is

$$\sigma_s = \sigma_i + k_y d^{-1/2} \tag{6}$$

where  $\sigma_s$  is yield strength;  $d$  is mean grain size;  $k_y$  and  $\sigma_i$  are constants.

The strength of the alloy decreases with the growing of grains ( $d$ ). Furthermore, overburning may happen at a higher temperature, leading to the decrease of elongation. Higher solution temperature and longer time without overburning, recrystallization and growth of the grains make the level of solid solution supersaturation higher. So, the smaller size specimen will have higher level of solid solution supersaturation. And more aging hardening precipitates can precipitate during the aging treatment. This is in accordance with the results of the DSC analysis. 7000 series aluminum alloys are aging hardening alloys, whose properties are determined by the coherent or semi-coherent precipitates formed during aging treatment. So, it can be found that specimen II has a higher HB hardness than specimen I when they are treated with the same process. And the electrical conductivity of specimen I (17.0 MS/m) is higher than that of specimen II (16.5 MS/m) [20].

## 4 Conclusions

1) Temperature variation can be influenced by the specimen size. The heating and cooling rates of the large specimen I are less than those of the small specimen when solution treated in the same furnace. Large size specimens undergo low solution temperature and short time.

2) The densities of GP zones and  $\eta'$  phases of small specimen are higher than those of the large specimen, which is consistent with the properties of the alloys.

## References

- [1] XIONG Bai-qing, LI Xi-wu, ZHANG Yong-an, LI Zhi-hui, ZHU Bao-hong, WANG Feng, LIU Hong-wei. Novel Al-7.5Zn-1.65Mg-1.4Cu-0.12Zr alloys with high strength high toughness and low quench sensitivity [J]. The Chinese Journal of Nonferrous Metals, 2009, 19(9): 1539–1547. (in Chinese)
- [2] WANG Tao, YIN Zhi-min, SUN Qiang. Effect of homogenization treatment on microstructure and hot workability of high strength 7B04 aluminum alloy [J]. Transactions of Nonferrous Metals Society of China, 2007, 17: 335–339.
- [3] STLIER K, WARREN P J, HANSEN V, ANGENETE J, GJØNNES J. Investigation of precipitation in an Al-Zn-Mg alloy after two-step ageing treatment at 100 °C and 150 °C [J]. Materials Science and Engineering A, 1999, 270(1): 55–63.
- [4] GODARD D, ARCHAMBAULT P, AEBY-GAUTIER E, LAPASSET G. Precipitation sequences during quenching of the AA 7010 alloy [J]. Acta Materialia, 2002, 50: 2319–2329.
- [5] CHEN Kang-hua, LIU Hong-wei, LIU Yun-zhong. Effect of promotively-solutionizing heat treatment on the mechanical properties and fracture behavior of Al-Zn-Mg-Cu alloys [J]. Acta Metallurgica Sinica, 2001, 37(1): 29–33. (in Chinese)
- [6] ZHANG Xin-ming, HUANG Zhen-bao, LIU Sheng-dan, LIU Wen-hui, ZHANG Chong, DU Yu-xuan. Effects of two-stage solution on microstructures and mechanical properties of 7A55 aluminum alloy [J]. The Chinese Journal of Nonferrous Metals, 2006, 16(9): 1527–1533. (in Chinese)
- [7] WARNER T. Recently-developed aluminum solutions for aerospace applications [J]. Materials Science Forum, 2006, 519–521: 1271–1278.
- [8] LIU J. Advanced aluminum and hybrid aerostructures for future aircraft [J]. Materials Science Forum, 2006, 519–521: 1233–1238.
- [9] LI Nian-kui, L (Ü) Xin-yu, CUI Jian-zhong. Effect of processing way and aging treatment on properties and microstructures of 7B04 aluminum alloy [J]. Transactions of Nonferrous Metals Society of China, 2008, 18: 541–547.
- [10] DESCHAMPS A, BRÉCHET Y. Nature and distribution of quench-induced precipitation in an Al-Zn-Mg-Cu alloy [J]. Scripta Materialia, 1998, 39(11): 1517–1522.
- [11] ROBINSON J S, CUDD R L, TANNER D A, DOLAN G P. Quench sensitivity and tensile property inhomogeneity in 7010 forgings [J]. Journal of Materials Processing Technology, 2001, 119: 261–267.
- [12] DUMONT D, DESCHAMPS A, BRÉCHET Y, SIGLI C, EHRSTRÖM J C. Characterisation of precipitation microstructures in aluminium alloys 7040 and 7050 and their relationship to mechanical behaviour [J]. Materials Science and Technology, 2004, 20: 1–10.
- [13] ASTM E92—82. Standard test method for Vickers hardness of metallic materials [S].
- [14] ASTM B557—84. Standard methods of tension testing wrought and cast aluminium and magnesium alloy products [S].
- [15] MUKHOPADHYAY A K, YANG Q B, SINGH S R. The influence of zirconium on the early stages of aging of a ternary Al-Zn-Mg alloy [J]. Acta Materialia, 1994, 42(9): 3083–3091.
- [16] RIONTINO G, DUPASQUIER A, FERRAGUT R, IGLESIAS M M, MACCHI C, MASSAZZA M, MENGUCCI P, SOMOZA A. Formation and Morphology of Hardening Nanostructures in an AlZnMg alloy [C]/NIE J F, MORTON A J, MUDDLE B C. Proceedings of the 9th International Conference on Aluminium alloys. Australia: Institute of Materials Engineering Australasia Ltd, 2004: 652–658.
- [17] LIM S T, YUN S J, NAM S W. Improved quench sensitivity in modified aluminum alloy 7175 for thick forging applications [J]. Materials Science and Engineering A, 2004, 371: 82–90.
- [18] ZENG Su-min. Disciplines of multiple factors affecting solution treating of aluminum alloy [J]. The Chinese Journal of Nonferrous Metals, 1999, 9(1): 1–13. (in Chinese)
- [19] DENG Yong-rui, XU Yang, ZHAO Qing. Phase transitions [M]. Beijing: Metallurgical Industry Press, 1996: 148. (in Chinese)
- [20] MONDOLFO L F. Aluminium alloys structure and properties [M]. London-Boston: Butter Worths, 1976: 25.

## AA7050 高强铝合金在固溶淬火过程中的 温度变化及固溶制度

李培跃<sup>1,2</sup>, 熊柏青<sup>2</sup>, 张永安<sup>2</sup>, 李志辉<sup>2</sup>

1. 洛阳船舶材料研究所, 洛阳 471003;

2. 北京有色金属研究总院 有色金属材料及制备国家重点实验室, 北京 100088

**摘要:** 采用温度记录系统、组织观察、力学性能测试、电导率测试和 DSC 热分析研究 7050 高强铝合金固溶过程中的温度变化, 确定合理的固溶热处理制度。采用了 2 种不同尺寸规格的试样进行试验。研究表明, 在本试验条件下的固溶热处理过程中, 大尺寸试样固溶温度相对较低, 固溶时间较短, 导致合金中强化析出相的体积分数减少。对于尺寸为 25 mm×25 mm×2.5 mm 和 70 mm×60 mm×20 mm 的试样, 合理的固溶热处理制度分别为(480 °C, 30 min)和(480 °C, 90 min)。小尺寸试样中的 GP 区和  $\eta'$  相密度大于大尺寸试样中相应的密度, 这与合金性能测试的结果一致。

**关键词:** 铝合金; 试样尺寸; 固溶处理; 升温速率; 强化析出相

(Edited by YANG Hua)